Journal of Biotechnology 359 (2022) 161–175

Contents lists available at ScienceDirect

Journal of Biotechnology

journal homepage: www.elsevier.com/locate/jbiotec

Metabolic rewiring revealed by cell-specific rate analyses from nontargeted exometabolomics during simultaneous consumption of glucose and lactic acid in a CHO fed-batch process

Yu Luo [a], Johanna Vappiani [b], Keegan Orzechowski [a], Pramthesh Patel [a], Daniel Sevin [b], Juan Aon [a,*]

[a] Microbial & Cell Culture Development, GlaxoSmithKline R&D, 709 Swedeland Road, King of Prussia, PA 19406, USA
[b] Cellzome GmbH, GlaxoSmithKline R&D, Meyerhofstrasse 1, 69115 Heidelberg, Germany

ARTICLE INFO

Keywords:
CHO
Physiology
Metabolomics
Carnitines
Oxidative phosphorylation

ABSTRACT

Previously, we reported, based on an untargeted metabolomics, carnitine derivatives are part of a mechanism to overcome impaired mitochondrial functioning triggered by an acyl-group overflow in CHO cells. In this study, we analyzed the cell-specific rates of 24 selected metabolites using two metrics: correlation coefficients and root-mean-square deviations (RMSDs) between glucose-fed versus glucose/lactic acid-fed cultures. The time-course profiles of acetylcarnitine, adipoylcarnitine, glutarylcarnitine, glutamate, and succinate exhibited significant negative correlations between the two culture conditions. Based on RMSDs, seven carnitine derivatives, 3-hydroxy-methyl-glutarate, mevalonate, pyridoxamine-5-phosphate, succinate, and glycine were substantially different. The analyses from the two metrics reveal a distinctive rearrangement of rates from the following metabolic pathways: (*i*) high secretion rates of carnitines as part of the acyl-group removal, (*ii*) low secretion rates of succinate, related to the tricarboxylic acid cycle and the electron-transport chain, (*iii*) low secretion rates of pyridoxamine-5-phosphate – a co-factor for amino acid catabolism, transaminations, and transsulfuration, and (*iv*) increases in the consumption rates of glutamate and glycine, both used to produce glutathione. The rewiring in rates observed upon feeding lactic acid is best explained by the activation of pathways supporting homeostasis of acyl-groups and antioxidant synthesis, which are required for continuous proper functioning of oxidative phosphorylation.

1. Introduction

Evidence recently gathered from metabolic profiling of cancer cells, heart failure, and metabolic diseases is increasingly demonstrating the flexibility of a mammalian cell's metabolism to overcome mitochondrial dysfunction, oxidative stress, and inflammation. The identification of system mediators such as long-chain acylcarnitine factors (Ellis et al., 2000; Hunter et al., 2016) and carnitine as the "shuttle-molecules" in cancer cells (Console et al., 2020) has been accomplished using metabolic profiling as an ideal tool for filling knowledge gaps. However, characterizing mammalian cells metabolically is still a demanding task – primarily due to the complexity of regulatory systems (Mulukutla et al., 2014). The complexity of dysfunctional mechanisms is reflected by the patterns of biomarkers, which are implicated in various metabolic diseases (Adeva-Andany et al., 2017; Brass, 1994; Orsatti et al., 2021). The uncovering of biomarkers or environmental conditions that trigger fast growth in cancer cells is an active field of study.

Mitochondrial dysfunctionality and the elevated resistance to oxidative stress are common features among cancer cells. Those cellular functions – proper mitochondrial activities of the tricarboxylic acid (TCA) cycle and the electron-transport chain (ETC), and homeostasis of the intermediates for the antioxidant defense – are partially impaired to become cancer-specific vulnerabilities (Koppula et al., 2017). As antioxidant defenses a cell possesses, methionine, glutamic acid, and glycine play essential roles in the synthesis of reduced glutathione (Sanderson et al., 2019). Methionine as a sulfur-containing amino acid is catabolized and recycled in a series of metabolic pathways known as the methionine cycle, which is connected to the folate cycle to become part of the one-carbon metabolism (Sanderson et al., 2019). The interconnected methionine cycle, folate cycle, methionine salvage pathway,

* Corresponding author.
E-mail address: juan.c.aon@gsk.com (J. Aon).

https://doi.org/10.1016/j.jbiotec.2022.10.004
Received 23 April 2022; Received in revised form 9 September 2022; Accepted 4 October 2022
Available online 8 October 2022

transsulfuration with reduced glutathione synthesis, and polyamine metabolism are all tightly regulated, and one alteration in one node of this network can lead to a drastic dysfunction in cancer cells (Bistulfi et al., 2010; Corbin and Ruiz-Echevarría, 2016; Lyon et al., 2020).

Coenzyme A (CoA) and acyl-CoA are critical intermediates in cellular oxidative pathways, including fatty acid β-oxidation, carbohydrate and amino acid oxidation, the TCA cycle, and biosynthetic reactions such as De novo fatty acid synthesis and complex lipid synthesis, (Brass, 1994; Shi and Tu, 2015). Acyl-CoA intermediates function frequently as allosteric regulators of enzymes that control pathway fluxes. The intracellular content of CoA in different mammalian cells is relatively low, so a cell depends on the on-going turnover of reactions involving the CoA and acyl-CoA pools to maintain its CoA availability. Acetyl-CoA can be considered an indicator of a cell's nutritional state. Acetyl-CoA is generated in the mitochondria from the import of pyruvate, the oxidations of fatty acids and amino acids. When cells are not growing actively (under limited feeding of nutrients for example), acetyl-CoA is not accumulating and is mostly driven to oxidative phosphorylation (OXPHOS), which generates NADH, FADH, and CO_2 subsequently (Shi and Tu, 2015).

Our previous work showed the relation of glucose and lactic acid co-assimilation with the reduced secretion of ammonium by CHO cells (Eyster et al., 2020). Furthermore, we reported a comparison of the exometabolome of the CHO cells grown in fed-batch cultures between two experimental conditions – a control group with only glucose fed continuously versus an experimental group with lactic acid fed continuously on day 5 and onward (in addition to the glucose feeding) as described in Vappiani et al. (2021). The supply of extra lactic acid was intended to fuel OXPHOS as a means to achieving a positive impact on growth and/or productivity (Li et al., 2012; Templeton et al., 2013). Evidence provided from several ^{13}C flux studies showed that CHO cells rely heavily on the TCA cycle and OXPHOS to supply energy during the stationary phase to produce recombinant proteins. This metabolic phenotype is often associated with a shift from lactate production to lactate consumption (Ahn and Antoniewicz, 2013; Luo et al., 2012; Templeton et al., 2017). The increased fraction of labeled pyruvate directed to mitochondria leads to a significant enhancement of the net production of NADH, which is largely used for OXPHOS (Templeton et al., 2017). However, based on the isotopic-steady-state analysis from the ^{13}C labeled-glucose consumed by CHO cells in stationary phase, most of the amino acids are not biosynthesized de novo but are consumed from the fed medium for protein and energy production (Sengupta et al., 2011).

Using untargeted semi-quantitative exometabolomics, we reported an extensive release of tentatively metabolites annotated as acylcarnitine derivatives from CHO cells concomitantly with 3-hydroxymethyl-glutarate (HMG) and an activation of mevalonate synthesis after feeding lactate to the culture. Those acylcarnitines are present as surrogate metabolites of (*i*) fatty acid (FAA-acyl-CoA) β-oxidation, (*ii*) amino acid (R-ketoacyl-CoA) catabolism, and (*iii*) oxidative decarboxylation of pyruvate (Vappiani et al., 2021). The activation of the carbon-buffering system mediated by carnitines is part of a known mechanism in mammalian cells to overcome a limited TCA cycle capacity to assimilate those acyl-CoA groups and so maintaining the acyl-CoA:free-CoA ratio for its proper and continuous function (Vaz and Wanders, 2002; Reuter and Evans, 2012). Moreover, it was reported that carnitines play a protective role in mammalian cells against the oxidative stress-induced DNA damage (Berni et al., 2008) and preventing the non-enzymatic acetylation of the mitochondria proteome by removing the acetyl groups (Davies et al., 2016). When the fed lactic acid was assimilated, the resulting mitochondrial dysfunction reverberated into the upstream pathways, producing an overflow of pyruvate due to the lack of its consumption by mitochondria; this explains the increase in the excretion of alanine too (Eyster et al., 2020). These results constitute evidence of a highly regulated TCA cycle, as most of their intermediates were kept at similar levels between treatments, despite an increased availability of pyruvate (Vappiani et al., 2021).

In this study, we identify the rewiring of metabolic pathways because of feeding CHO cells with lactic acid, based on an analysis of the changing patterns of the cell-specific metabolic rates from the data reported in Vappiani et al. (2021). Specifically, such rewiring affects the metabolism of carnitines, the functioning of the TCA cycle, and the glutathione synthesis as part of the antioxidant defense, causing prominent changes in the consumption rates of succinic acid, glutamic acid, and glycine, and substantial changes in the relative abundance of methionine, all of which we consider surrogate markers for the metabolomic pathways that are activated to maintain proper TCA cycle functions, in response to the perturbance introduced by the additional lactic acid.

2. Materials and methods

2.1. Media and cell culture

The details of the model cell line and the fed-batch process conditions used in this study can be found in Eyster et al. (2020). Specifically, a chemically defined proprietary nutrient feed was added in boluses on days 0, 3, 6, 8, 10, 12, and 14. Two glucose/lactic acid feeding strategies were tested: (1) glucose controlled at 4 g/L based on the measurements from Raman spectroscopy (N = 4), and (2) lactate controlled at 2 g/L and glucose controlled at 4 g/L via Raman, too (N = 3). An automated delivery of stock 2.5 M lactic acid and/or 300 g/L glucose was determined by the output of Raman spectroscopy coupled with a chemometric model designed to predict in situ glucose and lactic acid concentrations – the controllers adjusted the pump flow rates continuously to track the glucose and lactate concentration setpoints. All reactors were terminated after 17 days.

2.2. Offline analysis

Samples were collected daily for the measurement of cell concentration and viability (Vi-Cell XR, Beckman Coulter, Pasadena CA), pH/dissolved oxygen (DO)/dissolved CO_2 (dCO_2) (RapidLab 248 Blood Gas Analyzer, Siemens, Germany), and osmolality (A_2O, Advanced Instruments, MA, USA). Samples were taken typically before feeding as described in Vappiani et al. (2021). One set of daily filtered supernatants were sent to Cellzome GmbH and used for exometabolomics analysis (GlaxoSmithKline R&D, Meyerhofstrasse 1, 69117 Heidelberg, Germany). The samples for exometabolomics analysis were taken on days 0, 5, 7, 10, 13, 15, and 17 and were prepared by a 3-min centrifugation at 13,300x*g* and 4 °C, followed by a second centrifugation of 0.7 mL aliquots of supernatant using 0.2-micron Spin-X tubes at 13,300x*g* and 4 °C.

2.3. Untargeted metabolomics analysis by mass spectrometry

An untargeted metabolomics analysis was performed using the platform described in Vappiani et al. (2021). In brief, the pipeline aligns and averages scans of each individual file, then aligns spectra across all files in the dataset, performs centroiding and peak binning, re-calibrates the mass axis based on the above lock masses, and finally assembles a consolidated matrix of ion intensities. Detected ions were annotated as metabolites tentatively by matching known molecular masses within a tolerance of 5 mDa using the Human Metabolome database (Wishart et al., 2018) as a reference, considering [M-H] and [M-2 H] (negative mode) or [M+], [M+H], [M+Na] and [M+K] (positive mode) ions and up to two ^{12}C to ^{13}C substitutions. Using this approach, we can identify metabolites with identical chemical formula, or within the 5 mDa annotation tolerance. In our interpretations, we were conservative and focusing on metabolites that are known to be highly abundant or part of conserved metabolic pathways. Also, when multiple ions responding to a change in the feeding strategy were mapped to a shared pathway, we

favored the more parsimonious explanation over the alternative and less likely scenarios where multiple distant pathways were involved.

2.4. Analysis of rates from exometabolomics data

2.4.1. Data processing and estimation of cell-specific reaction rates of consumption or production

The raw data of metabolite ion (each metabolite ion identified based on the molecular mass as described in Vappiani et al., 2021) intensity values underwent a series of processing procedures before we could use them to estimate the cell-specific rates of metabolite ion consumption and production. For clarification, every metabolite ion is referred as a metabolite. For clarification, reaction rates of production can also be referred as secretion rates, and reaction rates of consumption can also be referred as uptake rates. For the i^{th} metabolite from the j^{th} experimental batch, there are seven time points, i.e., days 0, 5, 7, 10, 13, 15, and 17. The measured intensity values are represented by a vector, $\left[y_{i,j}(t_1),\ldots,y_{i,j}(t_7)\right]$, where $t_1 = 0,\ldots,t_7 = 17$ (see Vappiani et al., 2021 for the intensity values on a $\log_{10}$ scale, which were converted back to their original linear scale here and represented by $y_{i,j}$). The first processing step was subtracting the initial value, $y_{i,j}(t_1)$, from each value so that every time series starts at 0.

$$\bar{y}_{i,j}(t) = y_{i,j}(t) - y_{i,j}(t_1) \tag{1}$$

The second step was removing the day 0 values from each time series (i.e., baseline shift) and keeping the data from day 5 and onward (i.e., truncation). The rationale is that the process conditions of treatment B (without lactic acid feed, as the control condition) and treatment A (with lactic acid feed, as the experimental condition) started to diverge only on day 5 (therefore, the processes up to day 5 can be considered biological replicates). In addition, the estimated rates based on the data between day 0 and day 5 are subject to higher uncertainty due to the low cell counts and the measured intensity values closer to their detection limits, and these noisy estimates may skew the scale of a time series, which is critical to the calculation of the relative cell-specific rates in the next section.

Subsequently, the baseline-shifted and truncated data were further processed using smoothing splines. A piecewise cubic spline curve was fitted such that at each original data point the curve is smooth, and the cubic spline parameters were determined by balancing between goodness of fit and roughness. Doing so allowed us to have evenly spaced time series and estimate the first-order derivative of each time series. Each time series, $\bar{y}_{i,j}(t_2),\ldots,\bar{y}_{i,j}(t_7)$, was converted to an equal-distance series with a step size of ¼ days, using the "fit" function in MATLAB with the "smoothingspline" configuration (MATLAB R2020b). The tunable smoothing parameter was selected automatically based on the average spacing of the data points. The equal-distance time series is represented by a vector, $\left[\tilde{y}_{i,j}(s_1),\ldots,\tilde{y}_{i,j}(s_N)\right]$, where $s_1 = 5$ and $s_N = 17$. Each time series has N equally distanced data points. Similarly, the measured viable cell concentration (VCC) values were also approximated using smoothing splines, denoted by $\left[\tilde{x}_{v,j}(s_1),\ldots,\tilde{x}_{v,j}(s_N)\right]$, where "v" stands for VCC.

The cell-specific consumption or production rates of each metabolite were approximated by numerical differentiation in Eq. (2).

$$\widehat{\mathrm{CSR}}_{i,j}(s_k) = \frac{\tilde{y}_{i,j}(s_{k+1}) - \tilde{y}_{i,j}(s_k)}{s_{k+1} - s_k}\frac{1}{\tilde{x}_{v,j}(s_k)} \tag{2}$$

The average cell-specific rates (CSRs) were estimated for each treatment group per metabolite in Eq. (3).

$$\overline{\mathrm{CSR}}_{i,m}(s_k) = \frac{1}{|T_m|}\sum_{j\in T_m}\widehat{\mathrm{CSR}}_{i,j}(s_k) \tag{3}$$

The set T_m represents the collection of batches in treatment m (i.e., treatment A or treatment B); $|T_m|$ represents the number of batches in treatment m. Fig. 1 shows an example of the metabolic pathway of glycolysis, specifically two metabolites, e.g., glycerol and glycerol 3-phosphate (tentatively identified by their molecular masses). The panel A of Fig. 1 is from Vappiani et al. (2021), where the curves are linear interpolations of the average log10 intensity values; the panel B shows their corresponding CSRs from day 5–17. In panel A and panel B, orange is for treatment A, and blue is for treatment B. Panel C shows a representation of the metabolic pathway of glycolysis, the synthesis of glycerol 3 phosphate (Gly-3P) and glycerol, and the synthesis of lactate from pyruvate.

2.4.2. Relative average cell-specific rates

For each metabolite, its average CSRs in treatment A and treatment B were scaled such that the max production/consumption rate of both treatments was scaled to 100 % (production) or − 100 % (consumption). The nature of the untargeted LC/MS method prevents us from generating meaningful comparisons across metabolites as signal intensity does not equate concentration. By scaling the rates to the maximum of each metabolite, we could eliminate such an effect and compare the *trends* on the same scale instead of the absolute magnitudes of cell-specific rates among different metabolites.

$$\bar{\mathrm{CSR}}_{i,m}(s_k) = \frac{\overline{\mathrm{CSR}}_{i,m}(s_k)}{\max\limits_{m\in\{A,B\},k\in\{1,\ldots,N\}}\left|\overline{\mathrm{CSR}}_{i,m}(s_k)\right|} \times 100\% \tag{4}$$

2.4.3. Between-treatment correlation of relative cell-specific rates

The Pearson linear correlation coefficient, r_i, of the ith metabolite was calculated from the pair of N relative CSRs – one from treatment A and one from treatment B. A positive correlation coefficient implies that the relative CSRs in treatment A and treatment B are similar in terms of the general trend – for example, the relative CSRs are both rising in treatment A and treatment B. A negative correlation coefficient implies that the relative CSRs are opposite – when one rises, the other declines. Note that correlation coefficients are scale independent. That is, the relative CSRs of treatments A and B could differ greatly in magnitude, but they trend similarly, generating a positive correlation coefficient.

2.4.4. Between-treatment root-mean-square deviation of relative cell-specific rates

A "distance"-based metric was used to quantify the deviation in magnitude in a metabolite's relative CSRs from treatment B to treatment A. Such a "distance" was calculated using the root-mean-square deviation (RMSD) of a metabolite's relative CSRs between treatment A and treatment B. Unlike Pearson's r, RMSD depends on the difference in magnitude besides trend. To completement Pearson's r, RMSD was used to identify metabolites with substantial changes between treatments based on the absolute deviation in rate magnitudes. Using both metrics, we aim to identify the CSR profiles that trend in opposite directions, differ substantially in magnitude, or both.

$$\mathrm{RMSD}_i = \sqrt{\frac{\sum_{k=1}^{N}\left(\bar{C}\,\bar{SR}_{i,A}(s_k) - \bar{\mathrm{CSR}}_{i,B}(s_k)\right)^2}{N}} \tag{5}$$

3. Results

Based on a comprehensive semi-quantitative and time-dependent analysis of the exometabolome of CHO cells utilizing the extra lactic acid fed, we uncovered several carnitine derivatives as biomarkers of the simultaneous activation of TCA cycle anaplerotic pathways and a carbon-buffering pathway. The CHO cells that we studied exhibited a balance between intermediates from (*i*) amino acid catabolism, (*ii*) fatty acid β-oxidation, and (*iii*) pyruvate oxidative decarboxylation, and their carnitine derivatives. In addition, HMG and mevalonate syntheses were

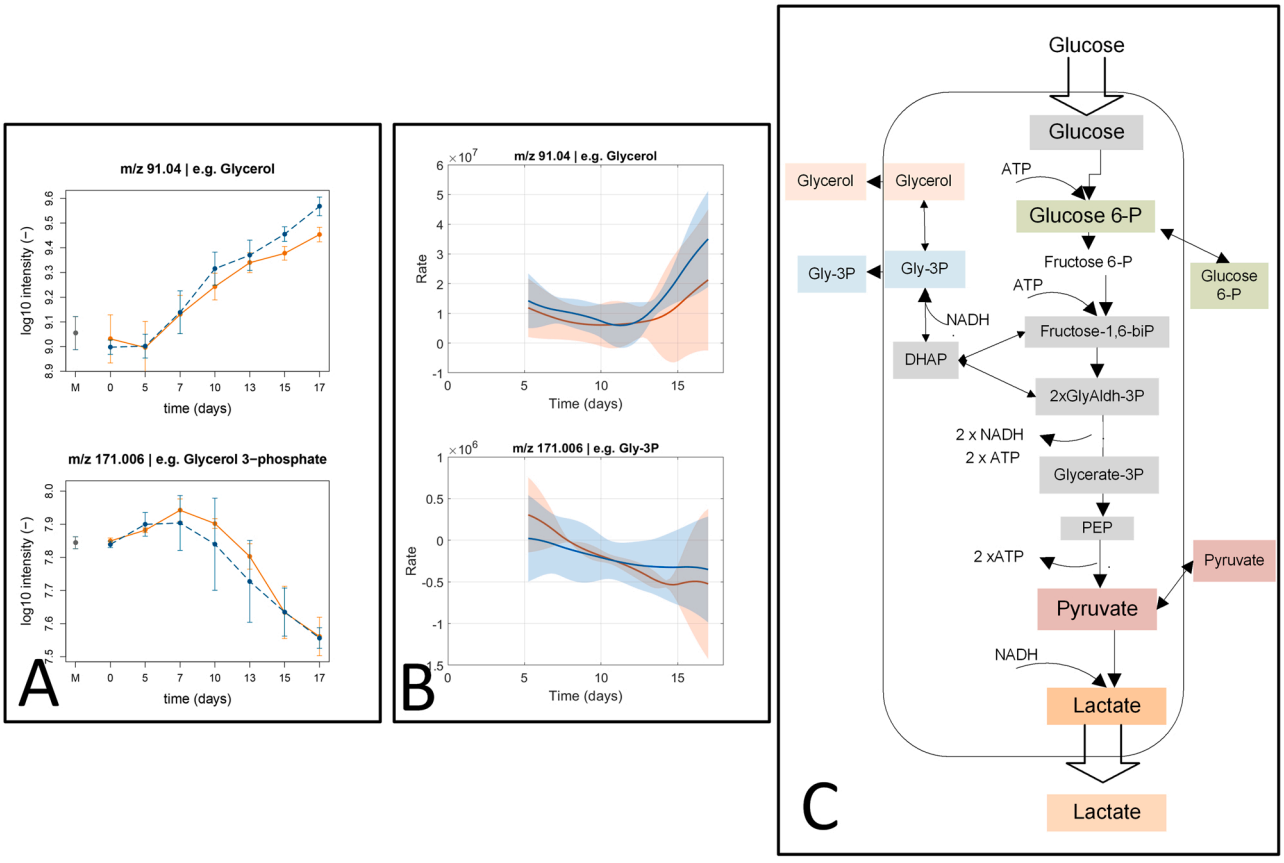

Fig. 1. Examples of intensities and computed cell-specific rates of two metabolites – glycerol and glycerol 3-phosphate. Panel A shows the intensities of glycerol and glycerol 3-phosphate (Gly-3P) versus time in days. Data are shown as mean and standard deviation of 3 (Lactic acid feed treatment A– orange line) or 4 (Control treatment B– blue dashed line) replicate cultures. 6 replicates for the reference culture media (M) at day 0 (gray dot). Panel B shows Rates of these two metabolites based on smoothing splines versus time in days from day 5. Rate in the y-axis represents the average cell-specific rate (CSR) per metabolite. The CSR of each metabolite were approximated by numerical differentiation in Eq. (2) as described in materials and method section. Same approximation of CSRs by numerical differentiation is done from Figs. 2–6. The Rate of a metabolite can be positive indicating its production/secretion or negative indicating its consumption/uptake. While panel C is a representation of the metabolic pathway of glycolysis and glycerol synthesis. The colored areas associated with the lines (treatment A– orange and treatment B-blue) are based on the 95 % confidence intervals of the mean. The gray colored areas represent the overlap of the 95 % confidence intervals of the mean CSRs from both treatments.

found as biomarkers of the alternative acyl group removal. Together, under a limited capacity to assimilate the surplus of acyl-CoA groups as well as maintain the acyl-CoA:free CoA ratio for proper and continuous functioning of the TCA cycle, the CHO cells activate the carnitine-buffering system, HMG, and mevalonate pathways (Vappiani et al., 2021).

3.1. Metabolite selection background

We selected a few metabolites that are relevant to the scope of this study for an in-depth analysis. In our previous analysis in Vappiani et al. (2021), we identified metabolites with statistically significant intensity differences between treatment A (with lactic acid feed) and treatment B (control condition without lactic acid feed). Those include ions tentatively annotated as mevalonate, HMG, and intermediates of carnitine-buffering system. The acylcarnitines can be formed from the transfer of acyl groups from the corresponding activated acyl-CoA thioesters, which are synthetized from three main metabolic pathways, (*i*) pyruvate oxidation, (*ii*) fatty acid β-oxidation, (*iii*) and amino acid catabolism. Then, we selected the amino acids that are part of the amino acid catabolism and were not supplemented during fed-batch cultures (the intensity values are related to but not identical to the actual metabolite concentrations; if an amino acid was supplemented, we could not estimate its CSRs accurately using Eq. (2)). In addition, we considered the intermediates of two metabolic pathways, e.g., TCA cycle and glycolysis, biologically important to be included. We included both carbon-backbone pathways due to their direct involvement in the assimilation of the two carbon sources, glucose, and lactic acid; therefore, we could evaluate whether the cell's homeostasis of both pathways resulted in a mitochondrial dysfunction.

3.2. Cell-specific rates of carnitine derivatives from both experimental conditions

To obtain an overview of the effect of lactic acid feeding on the carnitine-buffering system, we analyzed the time profiles of CSRs of all detected acyl carnitines. In Fig. 2, the average CSRs of nine acylcarnitines are shown as solid lines, colored by different experimental conditions (orange for treatment A and blue for treatment B). The shaded area represents the 95 % confidence intervals of the average CSRs per experimental condition. The lactic acid feed started on day 5 after cells exhibited the metabolic shift to the co-assimilation of lactate and glucose. Recall that in both treatment conditions, glucose concentration was controlled at 4 g/L while in treatment A, in addition, lactic acid concentration was controlled at 2 g/L through continuous supplementation of lactic acid as described in Materials and Methods.

There are clear separations in the time-course profiles of the acetylcarnitine, malonylcarnitine, glutarylcarnitine, adipoylcarnitine,

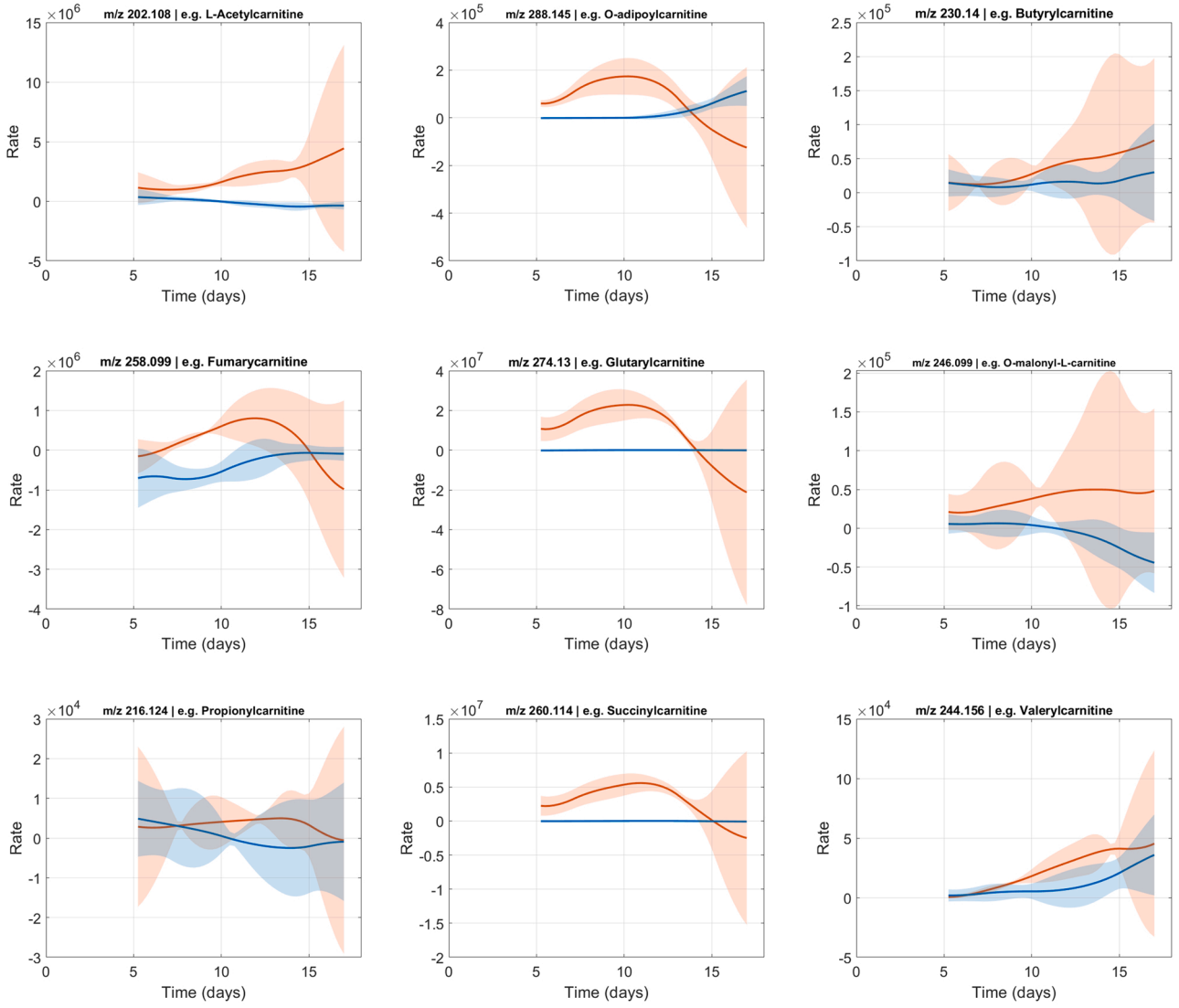

Fig. 2. Computed cell-specific rates of carnitine derivatives. Plots show the Rates estimated for control (blue line and area-treatment B) and Lactic acid feed (orange line and area-treatment A) per carnitine derivative with their corresponding colored-areas based on the 95 % confidence intervals of the mean. The gray colored areas represent the overlap of the 95 % confidence intervals of the mean CSRs from both treatments.

fumarylcarnitine, butyrylcarnitine, and succinylcarnitine when cells started consuming extra lactic acid during simultaneous glucose assimilation. Between treatments A versus B, the difference in averages of acetylcarnitine and malonylcarnitine CSRs increased 6-fold from day 5–17. The butyrylcarnitine CSRs were trending similarly to the CSR profiles of acetylcarnitine and malonylcarnitine when cells were co-fed with glucose and lactic acid (treatment A). However, between treatments A versus B, the difference in averages of butyrylcarnitine CSRs increased more than 80-fold between days 5 and 17. In the case of fumarylcarnitine, glutarylcarnitine, succinylcarnitine, and adipoylcarnitine, maxima in CSRs between days 10 and 13 were found in the cultures fed with glucose and lactic acid (treatment A). Between treatments A versus B, the difference in averages of fumarylcarnitine, glutarylcarnitine, succinylcarnitine, and adipoylcarnitine CSRs increased 1.9-fold, 2.1-fold, 2.5-fold, and 2.8-fold, respectively, from day 5 until those maxima (Fig. 2). The time-course profiles of propionylcarnitine and valerylcarnitine CSRs did not show a clear separation between treatments A and B.

In general, all nine carnitine derivatives either accumulated significantly or trended higher in the condition with lactic acid feed when compared with the control fed-batch cultures. The extra lactic acid feed brought higher secretion rates, reflecting the excess in the intracellular milieu of the corresponding acyl-CoAs generated from oxidative processes of pyruvate, amino acids, and fatty acids. In addition, under this situation of lactic acid feed where a large secretion of carnitine derivatives occurred, cells were expected to fulfill the high L-carnitine demand by increasing its endogenous synthesis. L-carnitine is produced from the amino acid precursors lysine and methionine, with lysine providing the backbone and those being methylated by S-adenosylmethionine (SAM), which is provided by methionine. In the mitochondria, per molecule of L-carnitine, there is a concurrent generation of one molecule of glycine, one molecule of NADH, and two molecules of succinic acid (Reuter and Evans, 2012). Succinic acid and carbon dioxide are generated from α-ketoglutarate via two dioxygenases consuming oxygen (Reuter and Evans, 2012; Adeva-Andany et al., 2017).

3.3. *Cell-specific rates of selected amino acids during fed-batch cultures under both experimental conditions*

To obtain an overview of the impact of feeding extra lactic acid on the metabolism of the three amino acids that were not fed periodically

during the fed-batch cultures, we analyzed the time profiles of the CSRs of glutamic acid, glycine, and alanine. Fig. 3 shows the plots of their CSRs versus time in days starting from day 5 for both experimental situations. Alanine and glutamic acid were in the basal medium from day zero. Glycine was not present either in the basal medium or in the feed medium. Previously, we reported alanine as a biomarker of pyruvate leak from the cells via transamination reaction catalyzed by the alanine amino transferase, ALT, where glutamic acid participates as the donor of amino groups to become α-ketoglutarate (Eyster et al., 2020).

There is a clear separation in the CSR profiles of glutamic acid and alanine from day 10 until the end of cultures. The glycine profiles show a separation from day 5–12; however, the separation is not statistically significant.

Starting on day 10, in the cultures fed with extra lactic acid, glutamic acid was consumed, and alanine was secreted at higher rates than those observed in the control cultures. This resulting pattern can be explained by the on-going transamination reactions where both amino acids were involved.

Glycine was produced during the first 5 days, and later its production rate decreased to very low levels until the end of both culture conditions. An active aerobic glycolysis (Warburg phenomenon) in the early 5 days generated serine and glycine from glyceraldehyde 3-phosphate, but later the metabolic shift to lactate consumption induced a lower glycolytic flux as reflected in lower glucose uptake rates (Eyster et al., 2020), causing the drop in production of glycine.

A common feature of the CSR profiles of glycine and glutamic acid is the low production at the onset of glucose and lactic acid co-assimilation, followed by a switch to consumption from day 8 for glycine, and day 10 for glutamic acid (Fig. 3). Based on the high secretion rates of several acylcarnitines especially from days 5–10 (after the lactic feed started) in Fig. 2, we expected to find higher production rates of glycine as part of the increasing synthesis of L-carnitine to compensate for a large demand from the cells. A possible retention of glycine from day 5 could be explained by demand from the cells to cover other biosynthetic processes such as reduced glutathione synthesis. Glutamic acid produces α-ketoglutarate via the enzyme glutamate dehydrogenase (GDH), so becoming one of the sources of succinic acid via succinate dehydrogenase (SDH) – the complex II and common catalytic step between the TCA cycle and ETC. Then, the high demand of glutamic acid could support, via the TCA cycle and ETC, the maintenance of the acyl-CoA:free-CoA ratio for the proper and continuous function of OXPHOS.

3.4. *Cell-specific rates of four TCA cycle intermediates from both experimental conditions*

Herein, we analyzed the CSR profiles of key TCA cycle and ETC intermediates to provide an overview of the impact of feeding extra lactic acid on OXPHOS as part of the mitochondrial activities. Fig. 4 shows the CSR profiles of four TCA cycle intermediates – citric acid, malic acid, succinic acid, and fumaric acid. These four TCA cycle intermediates were not fed periodically; they were secreted to the extracellular medium by the cells during the fed-batch cultures.

The trends in Fig. 4 indicate a bifurcation of the profiles of succinic acid and fumaric acid from days 12 and 14 respectively because of the extra lactic acid. The temporal profiles of malic acid and citric acid do not show statistically significant differences between treatments A and B.

Herein, there is a common pattern of the CSR profiles of succinic acid and fumaric acid after days 12 and 14 respectively when both organic acids started being consumed. There is a connection between the time-course profiles of glutamic acid and succinic acid. Based on the high secretion rates of several acylcarnitines from lactic feed onset until the end of the cultures (Fig. 2), we found from day 10 a switch from net low production rates to increasing consumption rates (Fig. 4). As part of the mechanism to compensate for the large leak of L-carnitine from days 5–10, more consumption (lower production rates) of glutamic acid is expected to occur by supplying succinic acid via α-ketoglutarate synthesis (Reuter and Evans, 2012; Adeva-Andany et al., 2017). From days 5–10 during the large leak of L-carnitine, a high retention of succinic acid by cells was also seen in the significantly lower relative intensities in the lactic acid-fed cultures than those in control cultures (Vappiani et al., 2021). The changes of the CSRs of glutamic acid, succinic acid, and glycine can be seen more clearly in the relative CSRs (Eq. (4)) in Fig. 10. Then, in comparison with the control cultures, there were low relative production rates from day 5–10 when the cells were fed with lactic acid, implying the presence of two on-going key processes – i.e., reduced glutathione (GSH) production and active TCA cycle functioning. Both processes could be in response to the presence of oxidative stress in the early days of feeding lactic acid, which affected the proper functioning of OXPHOS. From day 10, the restoration of the proper functioning of OXPHOS could occur, based on the increased synthesis of the antioxidant GSH and the lower secretion of some acylcarnitines (Fig. 2).

3.5. *Cell-specific rates of glycolysis intermediates and byproducts from both experimental conditions*

We analyzed the CSR profiles of the secreted intermediates of glycolysis and glycerol synthesis as they are also part of CHO's central carbon metabolism. Fig. 5 shows two glycolysis key intermediates – glucose glucose-6 phosphate (Glc-6P) and pyruvic acid – and two from the glycerol biosynthesis pathway – glycerol-3 phosphate (Gly-3P) and glycerol, both considered byproducts in the NAD^+ supply to glycolysis. These metabolites were not fed periodically; they were secreted to the extracellular medium by the cells during the 17-day cultures.

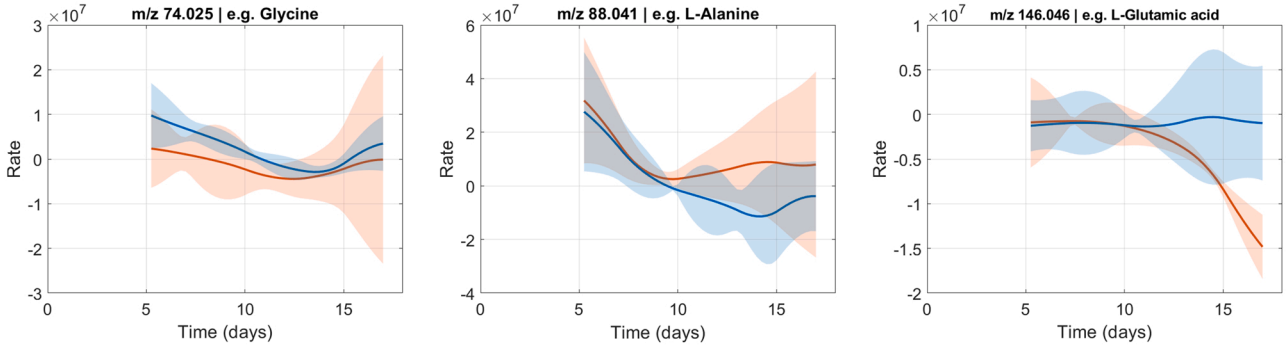

Fig. 3. Computed cell-specific rates of three amino acids – glycine, alanine, and glutamic acid. Plots show the Rates estimated for control (blue line and area-treatment B) and Lactic acid feed (orange line and area-treatment A) per amino acid with their corresponding colored-areas based on the 95 % confidence intervals of the mean. The gray colored areas represent the overlap of the 95 % confidence intervals of the mean CSRs from both treatments.

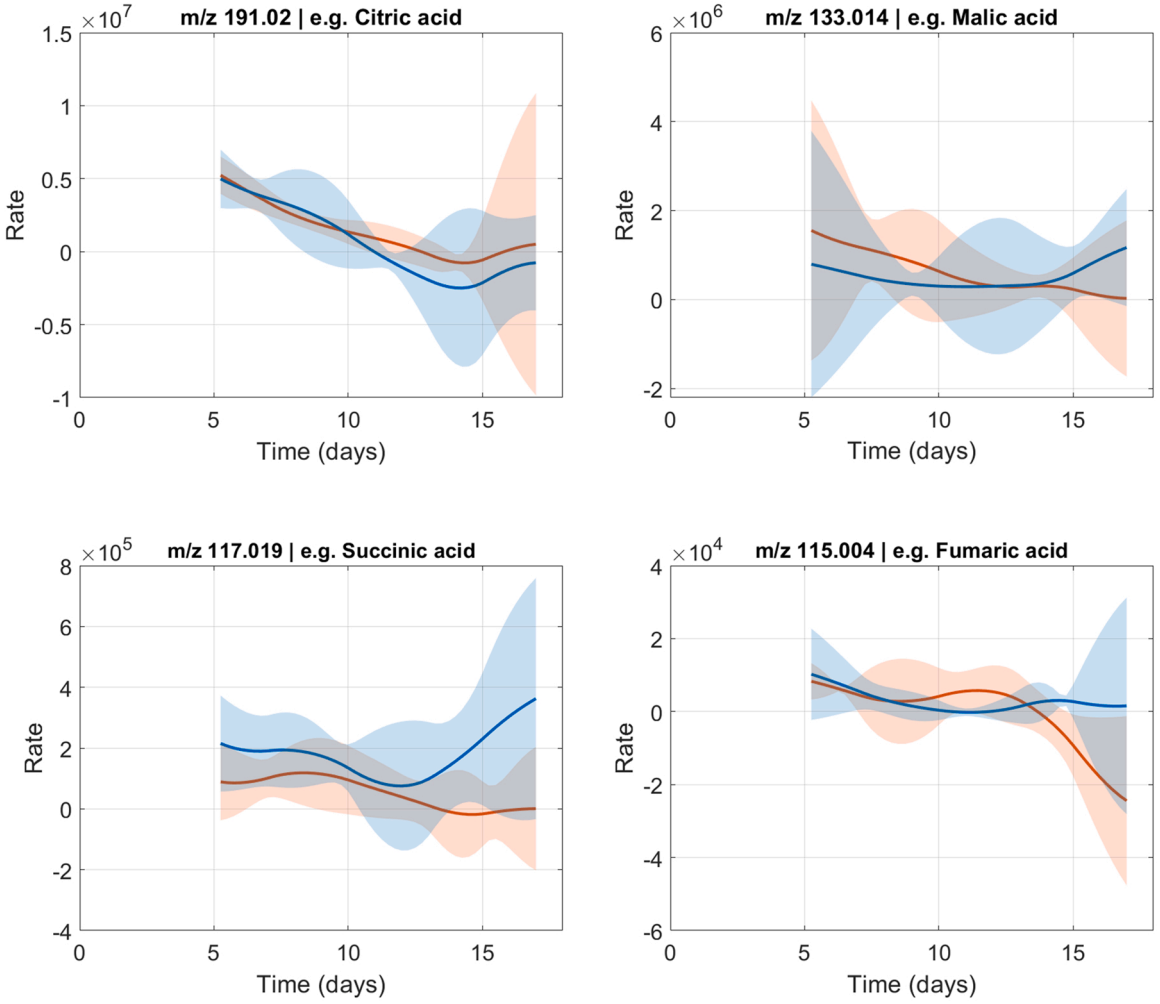

Fig. 4. Computed cell-specific rates of TCA cycle intermediates – citric acid, malic acid, succinic acid, and fumaric acid. Plots show the CSRs estimated for control (blue line and area-treatment B) and Lactic acid feed (orange line and area-treatment A) per TCA cycle intermediate with their corresponding colored-areas based on the 95 % confidence intervals of the mean. The gray colored areas represent the overlap of the 95 % confidence intervals of the mean CSRs from both treatments.

The temporal profiles of glucose-6P, gly-3P, glycerol, and pyruvic acid do not show statistically significant different rates between treatments A and B throughout the 17 days of culture. These results imply that the co-assimilation of lactic acid and glucose had no effect on glycolysis.

3.6. Cell-specific rates of mevalonate pathway intermediates, hydroxymethylglutaric acid, and co-factor pyridoxamine phosphate from both experimental conditions

We analyzed the CSR profiles of the intermediates of HMG and mevalonate syntheses, which were identified as biomarkers of the alternative acyl group removal in our previous work. Fig. 6 shows two mevalonate pathway intermediates – mevalonic acid and mevalonolactone – and 3-hydroxymethylglutaric acid (HMG). These metabolites participate cooperatively in the cellular mechanism of the acetyl-CoA removal via carnitine formation (Vappiani et al., 2021). Pyridoxamine-5 phosphate (PMP), an intermediate of the assimilation path of vitamin B6 pyridoxine, is a co-factor of the branch-chain amino acid transaminase (BCAT). Although PMP is considered here for the rate profiles versus time, the other intracellular intermediate pyridoxal-5 phosphate (PLP) does not show differences in the relative abundances between treatments A and B (control). The plots show their CSRs versus time in days starting from day 5 for both experimental situations.

The temporal profile of mevalonic acid diverge from day 9 onward; however, the trends of the other three metabolites show little differentiation in rates between treatments A and B throughout the 17 days of culture.

3.7. Analysis based on two analytical metrics to quantify metabolic rates changes

To compare CSRs between treatments A and treatment B among different metabolites systematically, we normalized their values shown in Figs. 2–6 to percentages relative to their respective maxima in both conditions (Eq. (4)) in Fig. 7.

3.8. Correlation analysis: opposite trends in time-course profiles of metabolic rates

We compared the relative CSRs between treatments A and B for each metabolite and ranked the metabolites based on their Pearson's r values in descending order (Fig. 8). r values that are not significant (i.e., $p > 0.1$) are not shown. There are five metabolites – O-adipoylcarnitine, acetylcarnitine, O-malonylcarnitine, succinic acid, and glutamic acid – with their CSRs trending generally in opposite directions when the cells co-metabolized lactic acid and glucose in comparison with just consuming glucose. The three carnitine derivatives were secreted rapidly from days 5–17, except that adipoylcarnitine was consumed in the last two days, when lactic acid was fed. We found that the rates of

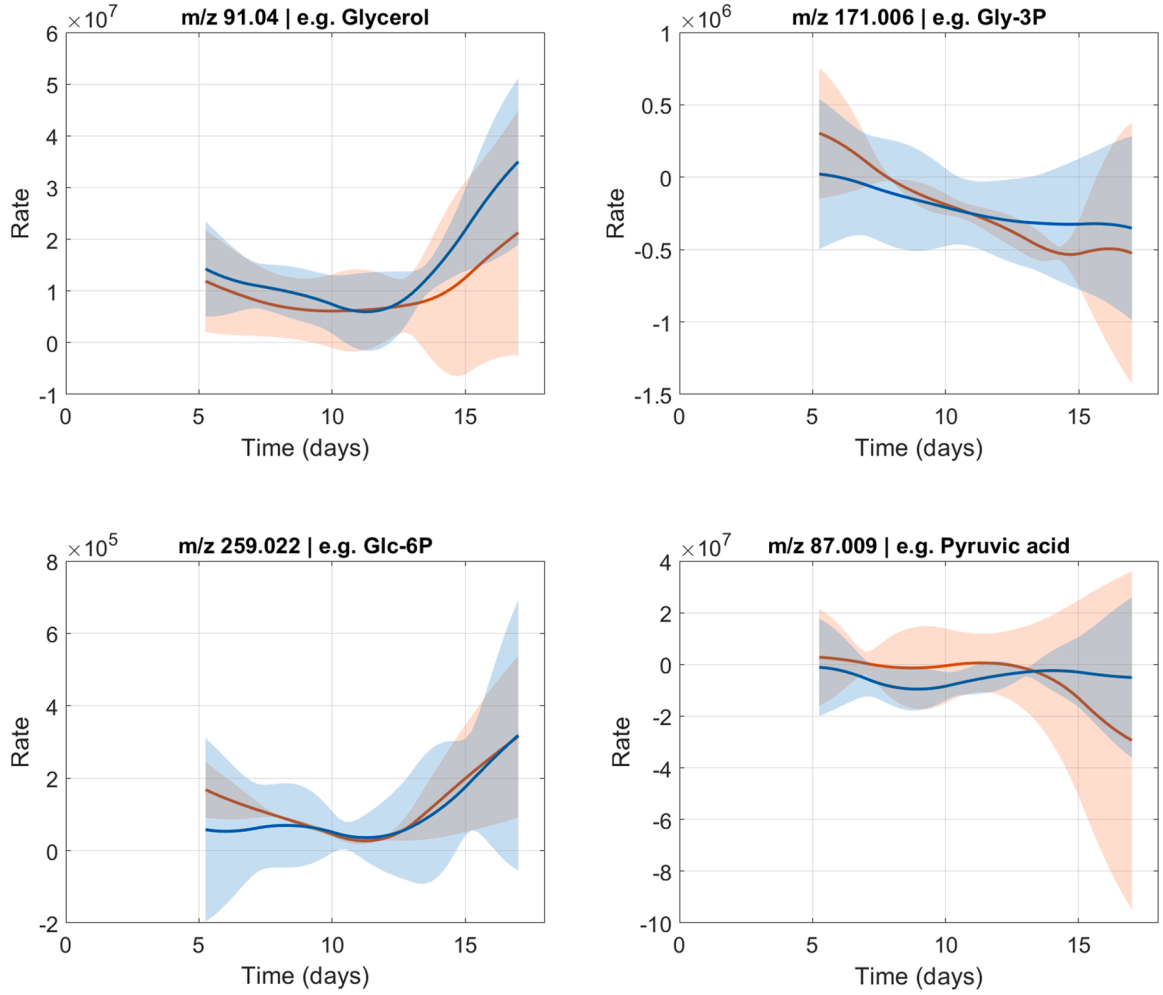

Fig. 5. Computed cell-specific rates of glycolysis and glycerol synthesis intermediates – glycerol, glycerol 3-phosphate, glucose 6-phosphate, and pyruvic acid. Plots show the CSRs estimated for control (blue line and area-treatment B) and Lactic acid feed (orange line and area-treatment A) of glycerol, Gly-3P, Glc-6P, and pyruvic acid with their corresponding colored-areas based on the 95 % confidence intervals of the mean. The gray colored areas represent the overlap of the 95 % confidence intervals of the mean CSRs from both treatments.

these three carnitine derivatives show a strong negative correlation between treatments A and B, specifically when the cells consumed lactic acid from day 5–17. In the case of acetylcarnitine and O-malonylcarnitine, when the cells consumed lactic acid, these two carnitines were secreted increasingly from day 5 to the end of the culture (Fig. 9) while the O-adipoylcarnitine secretion rates increased until day 10, and from that time point onward, the secretion rate started to decrease until day 15 when it turned into consumption with an increasing rate. The two carnitine derivatives represent the removal of the acetyl, and the malonyl groups directly appear to reflect their high intracellular availability when pyruvate was processed through the TCA cycle in the mitochondria. Malonyl groups were provided by Propanedioic (C3:0) acid. On the other hand, the adipoyl groups removal happened until day 10, and this C6-medium-chain carnitine derivative was re-taken to be fully oxidized in the mitochondria until day 17.

Now consider succinic acid, a key TCA cycle intermediate. The cells consuming only glucose showed high production rates of succinic acid, which increased from days 10–17 in comparison with those that co-assimilated glucose and lactic acid. This result indicates that when lactic acid is consumed by cells, it induces the retention of succinic acid. In connection with the lower succinic acid secretion rates, when the cells were assimilating lactic acid from days 10–17, a quick increase in the consumption rate of glutamic acid occurred simultaneously (Fig. 9). It is expected both succinic and glutamic acids to contribute to the proper functioning of the TCA cycle when an extra supply of pyruvate was provided from the oxidation of lactic acid. Succinic acid is a substrate for the respiratory-chain complex II succinate dehydrogenase (SDH) to produce fumaric acid and FADH. The α-keto-glutarate (α-KG), an intermediate of the TCA cycle (up-stream of SDH), is produced from glutamic acid via the step catalyzed by the glutamate dehydrogenase. Also, glutamic acid could be highly demanded for the transamination reactions and for the synthesis of GSH.

3.9. *RMSD analysis: significant separation in time-course profiles of metabolic rates*

While a negative correlation coefficient implies that the CSR trajectory turned to an opposite direction from treatment B to treatment A for a metabolite, it captures only a subset of metabolites that had substantial changes between treatments. Two CSR trajectories that follow a similar trend but differ greatly in magnitudes would yield a positive correlation coefficient. Fig. 9 shows two examples of propionylcarnitine and pyridoxamine 5-phosphate (pyridoxamine-5P) between treatments A and B. In the case of propionylcarnitine, the correlation coefficient was estimated to be not statistically significant (i.e., $p > 0.1$), but the rate profiles are visibly different, and they differ greatly in magnitude. Pyridoxamine-5P's time-course profiles exhibit a strong positive correlation based on the trends between experimental conditions (i.e., they

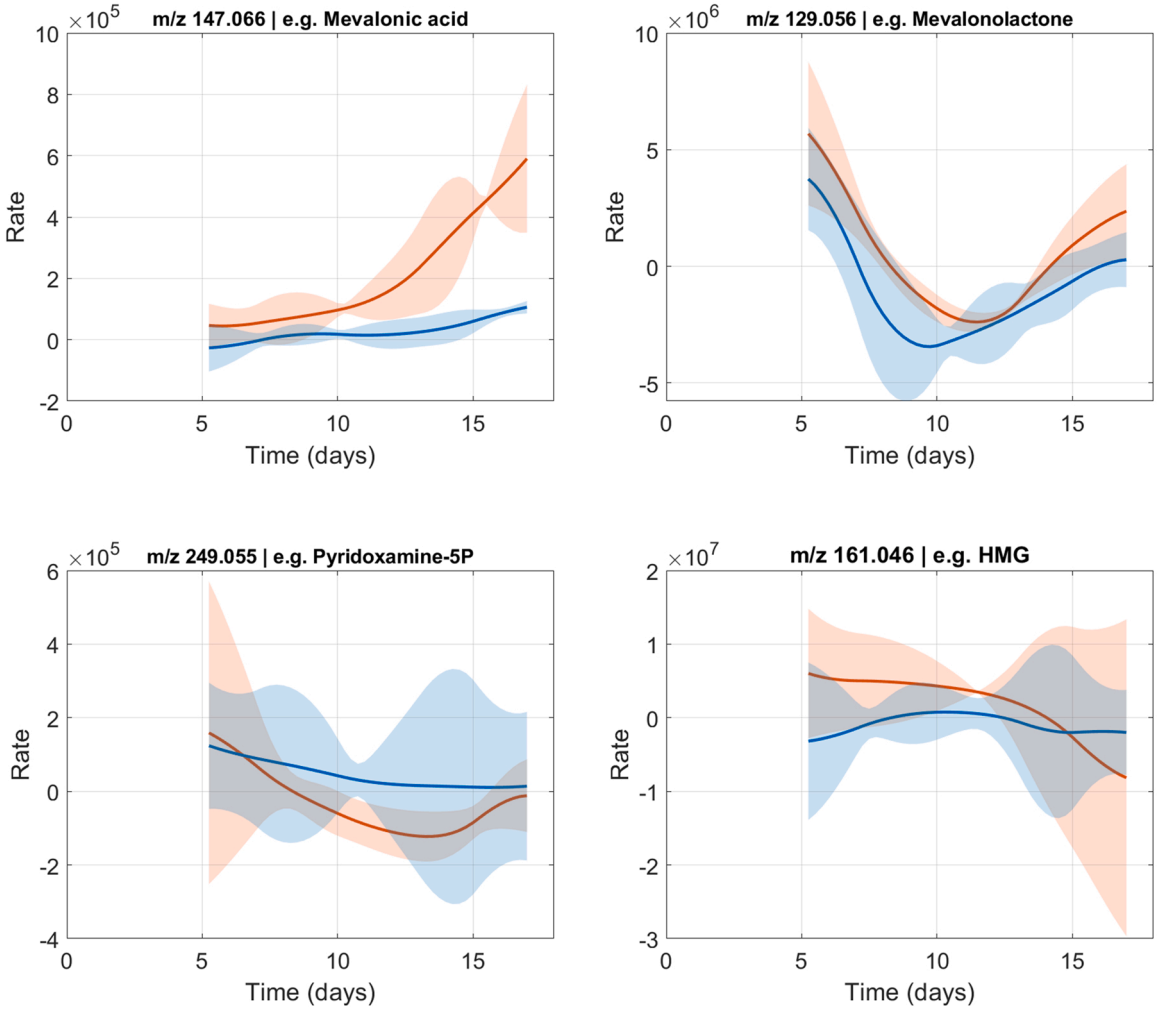

Fig. 6. Computed cell-specific rates of co-factor pyridoxamine 5-phosphate, 3-hydroximethlyglutaric acid, and two intermediates of mevalonate pathway such as mevalonic acid and mevalonolactone. Plots show the CSRs estimated for control (blue line and area-treatment B) and Lactic acid feed (orange line and area-treatment A) of every metabolite with their corresponding colored-areas based on the 95 % confidence intervals of the mean. The gray colored areas represent the overlap of the 95 % confidence intervals of the mean CSRs from both treatments.

trend similarly), but their orders of magnitude are not the same at any time points. To complement the identification of key metabolites through correlation coefficient, we used another metric, i.e., RMSD, to identify other differences in the rate profiles. We calculated the RMSD of the rate profiles between treatments for each metabolite to capture the significant changes in the magnitude of the metabolic rates at different time points.

Fig. 10 panel A shows the relative CSRs throughout the 17-day cultures including all 24 metabolites in the two experimental conditions – treatments B and A. Furthermore, we calculated the RMSD for each metabolite based on its relative rates between two treatments. Fig. 10 panel B shows the RMSD values ranked in descending order and colored in quartiles. The first quartile of six metabolites contains six carnitine – fumarylcarnitine, succinylcarnitine, glutarylcarnitine, O-adipoylcarnitine, propionylcarnitine, and O-malonylcarnitine. Within this group, three out of the six were already identified by the correlation analysis, the additional carnitine derivatives, succinyl-, glutaryl-, and fumaryl-carnitine, are directly related to the removal of their corresponding reactive species succinyl-CoA from the TCA cycle; glutaryl-CoA and fumaryl-CoA are derived from amino acid catabolism. The second quartile (with smaller RMSDs) contains acetylcarnitine, pyridoxamine-5 P, HMG, succinic acid, glycine, and mevalonic acid, considering that HMG mevalonic acid, and acetylcarnitine are in the pathways for the removal of the acetyl groups. The CSRs during the 17-day culture of succinic acid were identified by both metrics as significantly changed when the cells started consuming extra lactic acid. Pyridoxamine-5P rates also changed significantly, possibly suggesting the activation of amino acid catabolism, specifically of the branch-chain amino acids. When the cells assimilated extra lactic acid after day 5, glycine production rates were lower in comparison with the control condition (treatment B) followed by a constant uptake rate from day 7–15.

4. Discussion

The main purpose of this study is to understand CHO cell's re-wiring of metabolism when extra lactic acid is fed from day 5 onward. By examining an un-targeted CHO exometabolome, we report that the proper and continuous functioning of the TCA cycle was maintained after cell metabolism shifted to the co-assimilation of lactic acid and glucose. As a result of feeding the extra lactic acid, acyl-CoAs (including acetyl-CoA) were highly produced intracellularly, a carnitine-based carbon-buffering mechanism was triggered to keep proper mitochondrial activities of the TCA cycle and ETC by mitigating the surpluses of acyl-CoAs. Specifically, several acylcarnitine derivatives were found at elevated levels in the extracellular medium when the cells were fed with lactic acid compared with those that were fed with glucose alone. In addition, two other alternative pathways – the 3-hydroxy-methyl-glutaric acid (HMG) and mevalonate syntheses – appeared to be active to

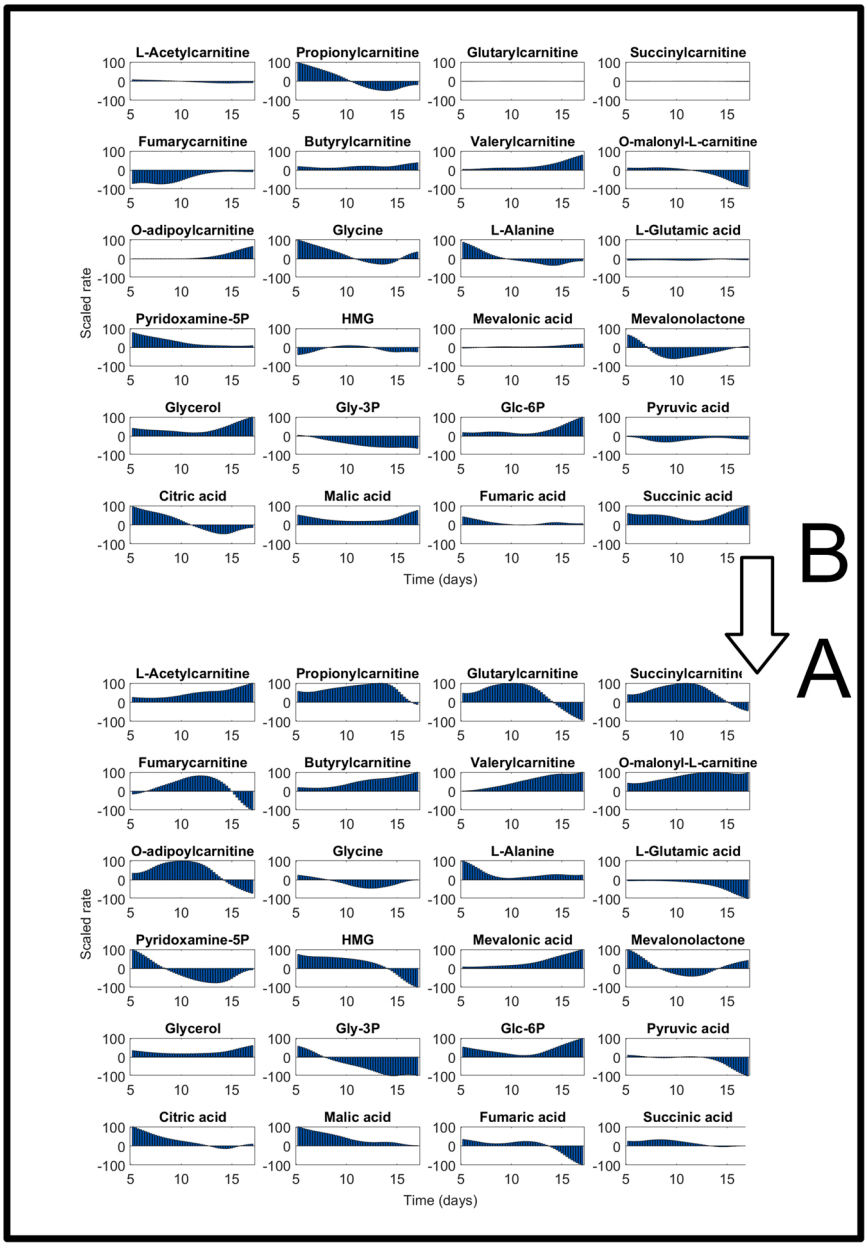

Fig. 7. Relative cell-specific rates of 24 metabolites. For each metabolite, its average CSR in treatment A (bottom tile-panel) and treatment B (top tile-panel) were scaled such that the maximum of consumption or production CSR of both treatments was scaled to 100 % (production) or 100 % (consumption).

manage specifically the acetyl-CoA surplus resulting from feeding the extra lactic acid. Here in, two metrics were used to elucidate the presence of oxidative stress based on the significant changes in the time-course profiles of 12 metabolic rates. Then, to keep the TCA cycle and ETC running properly while precluding the potential cellular damage by oxidative stress, the intermediates – glycine, glutamate, PMP – required for the antioxidant glutathione synthesis were found to be highly demanded by cells. In addition, under reduced glucose uptake rates when cells co-assimilated lactic acid (Table S7 in Vappiani et al., 2021), an expected reduction of the cytosolic redox pool of NADPH could compromise the ratio of reduced glutathione to its oxidized form (GSH/GSSG), and so affecting the antioxidant defense of the cells. Concomitantly, these results of high secretion rates of carnitine derivatives point to an overwhelmed TCA cycle capacity to process the extra acetyl groups from pyruvate oxidation. In addition, there were high cell-specific secretion rates of other acyl groups derived from fatty acid β-oxidation and amino acid catabolism. All results together explain CHO's possible metabolic adaptive response to the lowered antioxidant glutathione defense from day 5 with a subsequent onset of a negative impact on the TCA cycle enzyme activities, creating a partially reduced capacity of the TCA cycle to continue processing all acyl-CoAs from the three metabolic pathways – pyruvate oxidation, amino acid catabolism, and fatty acid β-oxidation.

This study was designed to test the hypothesis that feeding lactic acid as an extra supply of carbon could improve OXPHOS, and so to improve the energy supply for better growth and/or productivity (Li et al., 2012; Templeton et al., 2013). Furthermore, from ^{13}C labeled glucose studies in isotopic steady state at the stationary phase (non-growth phase), the TCA cycle intermediates, and citrate were not labeled, implying that a small fraction of pyruvate from the glycolytic flux was entering in the mitochondria (Sengupta et al., 2011). Consequently, under an active OXPHOS demanded by CHO cells during the stationary phase, the TCA cycle and ETC proper functioning might be sustained mainly by the contribution of intermediates, e.g., the acyl groups, from pyruvate

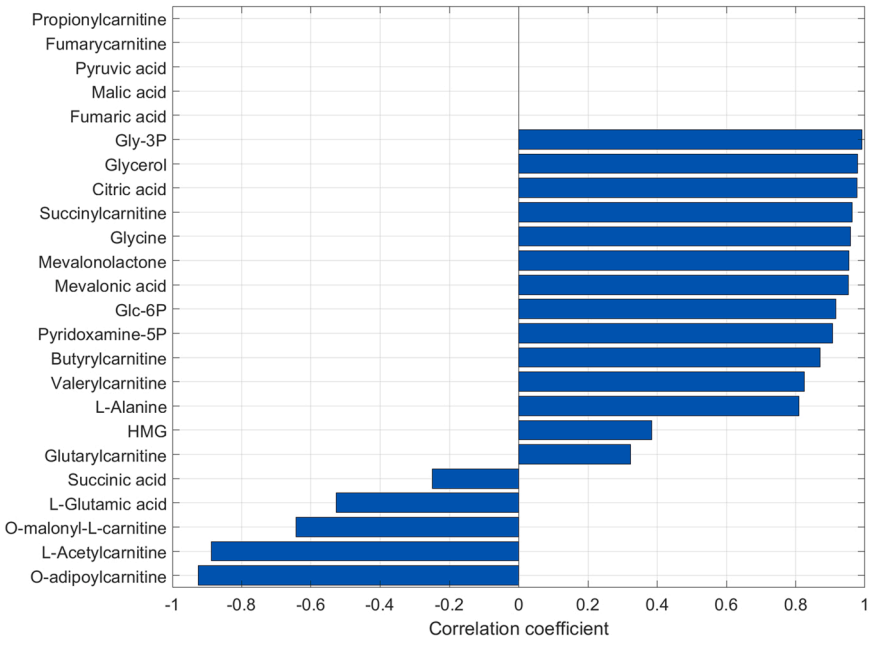

Fig. 8. Correlation analysis of the relative cell-specific rates of 24 metabolites. Relative CSRs between treatments A and B for each metabolite are ranked based on their Pearson's *r* values in descending order.

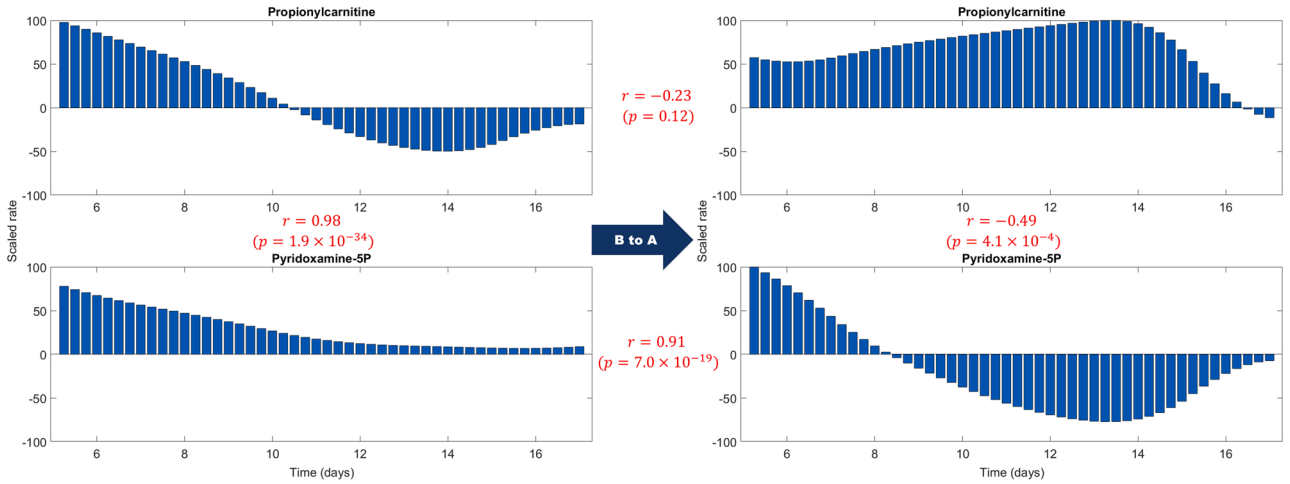

Fig. 9. Examples of different patterns of relative cell-specific rates of two metabolites – propionylcarnitne and pyridoxamine 5-phosphate – between treatments. Relative CSRs between treatments A (right plots) and B (left plots) for each metabolite. Plots show computed Pearson's *r* values and statistically significance based on *p* values per metabolite per treatment and between treatments.

channeled from lactic acid oxidation, from amino acid catabolism, and from fatty acid β-oxidation (Fig. 11). Then, we reported the challenging situation at the TCA cycle level in CHO cells to assimilate the carbon surplus from the lactic acid feed (treatment A). An intramitochondrial acetyl-CoA pool, maintained by the pyruvate dehydrogenase (PDH) activities from lactic acid consumption, could surpass the TCA cycle's native capacity to process all those acetyl groups in the first 5–13 days of a culture. Dealing with the TCA cycle's inability to process excess CoA derivatives, the CHO cells started using their carbon buffering mechanism based on carnitine, and additionally two pathways involving the syntheses of HMG and mevalonate to keep the homeostasis of acyl-CoA and a free CoA pool in the mitochondria.

The analysis of the relative CSRs of the 24 metabolites (Fig. 7) brought to us deeper insights into a cell's physiological condition to explain this overwhelmed TCA cycle capacity and the activation of the carbon-buffering system as reflected in the high secretion rates of seven acylcarnitines, HMG, and mevalonic acid. The analysis of the exometabolome revealed that several metabolic pathways were affected by the consumption of the extra lactic acid after day 5 when compared with the control condition of just controlling glucose to keep its concentration in the medium at 4 g/L. In our study, we analyzed a group of 24 metabolites that consist of nine acyL-carnitines (Fig. 2), three amino acids (Fig. 3), four TCA cycle intermediates (Fig. 4), two glycolysis pathway intermediates and two glycerol pathway intermediates (Fig. 5), and pyridoxamine-5P (PMP), a key co-factor for enzymes involved in transaminations, amino acid catabolism, and transsulfuration (Fig. 6). The rationale to have this group of selected metabolites is to include those that constitute the central carbon backbone of CHO cells (i.e., glycolysis, TCA cycle, ETC).

The two metrics used to compare CSR profiles between treatments show how the CHO cells adapted to a higher lactic acid uptake rate in treatment A than that in treatment B (Figs. 8 to 10). The significant

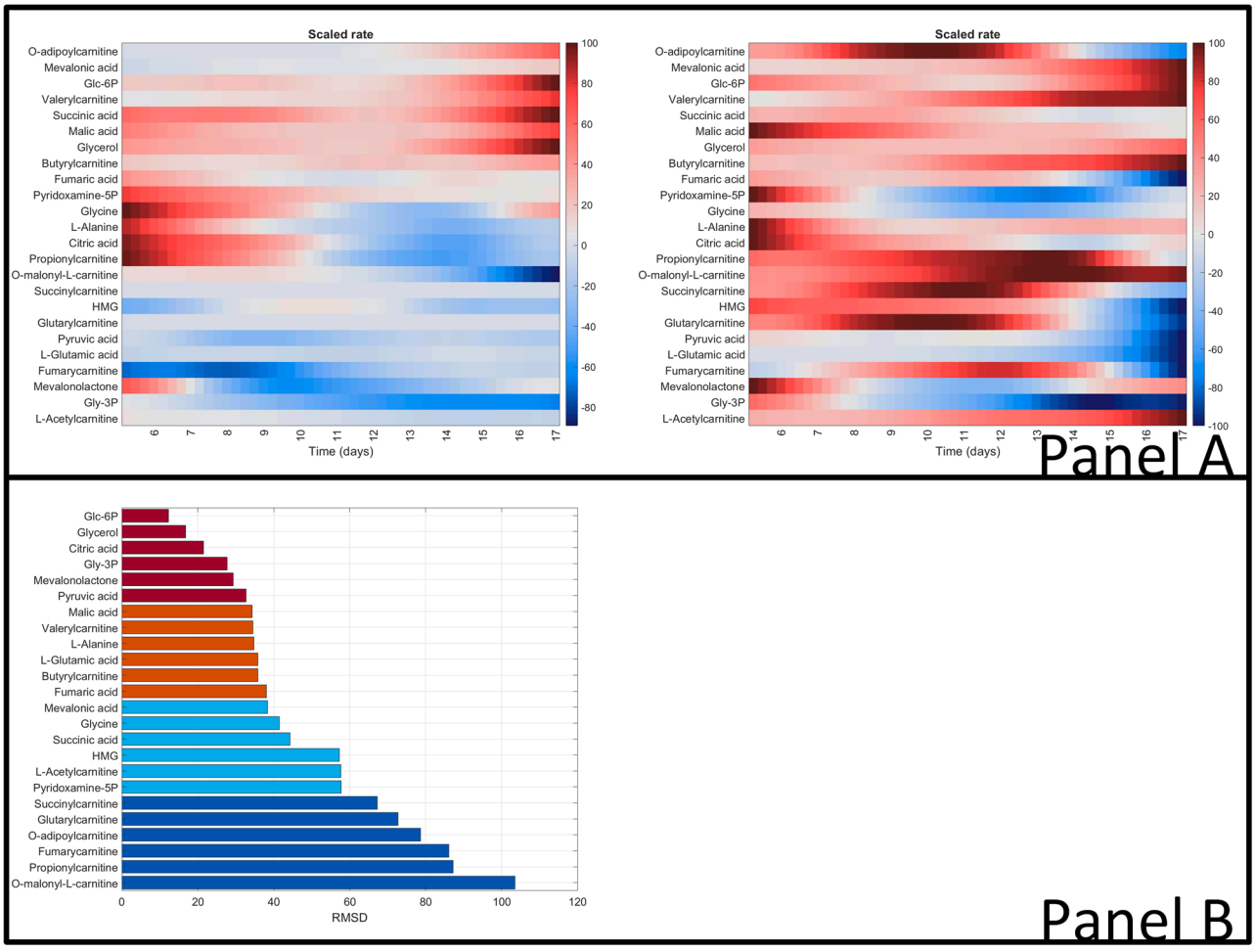

Fig. 10. RMSD analysis of the relative cell-specific rates of 24 metabolites. Panel A shows the relative CSRs throughout the 17-day cultures including all 24 metabolites in the two experimental conditions – treatments B (left panel) and treatment A (right panel) – in a heatmap with red indicating higher production rates and blue indicating higher consumption rates. Calculated RMSD for each metabolite based on its relative rates are shown panel B. RMSD values ranked in descending order and colored in quartiles. The first quartile of six metabolites (dark blue bars), second (light blue), third (orange), and fourth quartile (dark red).

changes in the time-course profile of such a key TCA cycle intermediate as succinic acid led us to infer an active TCA cycle and ETC functioning in response to the presence of oxidative stress. A large secretion of carnitine derivatives was possible by the increasing endogenous synthesis of L-carnitine (data not shown), concomitantly producing per L-carnitine molecule, one of glycine and two of succinic acid (Reuter and Evans, 2012). However, the cells exhibited a lower secretion rate of succinic acid when assimilating extra lactic acid from day 5 (Fig. 4) and a lower relative abundance of succinic acid than that in the control cultures (Fig. 5 in Vappiani et al., 2021). Succinic acid's lower secretion rates to the medium could be explained by its higher demand when the TCA cycle was actively assimilating those extra acyl-CoA groups via succinate dehydrogenase (SDH) – a unique enzyme connecting the ECT and TCA cycles. Then, from day 5–10, by the presence of oxidative stress, the TCA cycle and ETC could be partially impaired and so the carbon-buffering system was activated to overcome this limited processing capacity of acyl-CoA groups until the antioxidant levels of GSH were restored.

We also infer the induction of oxidative stress based on the significant changes in the CSR profiles of glutamic acid, glycine, and PMP, in addition to the low relative abundances of methionine reported in Vappiani et al., 2021. From days 7–15, the CHO cells exhibited higher consumption rates of those two none-fed amino acids, both of which are required for the synthesis of GSH. Evidence provided from ^{13}C labeled glucose studies in isotopic steady state at the stationary phase (non-growth phase) shows that CHO cells are diverting flux from glycolysis to produce large quantities of NADPH (Sengupta et al., 2011). The redirection of glucose 6-phosphate to the oxidative pentose-phosphate-pathway (PPP) might be demanded for the synthesis of fatty acids and steroids, or counteracting oxidative stress (Voet and Voet, 1995). Since CHO cells are not proliferating, the most probable function of this high NADPH synthesis is to counteract the presence of oxidative stress (Sengupta et al., 2011). CHO cells could increase by as much as 200-fold PPP activity via glucose-6-phosphate dehydrogenase in the presence of oxidative stress (Tuttle et al., 2000). Furthermore, in Young's review (2013) that describes a dynamic flux rewiring, CHO cells exhibit: (*i*) a drop in the specific glucose consumption rate, (*ii*) an upregulation of the oxidative PPP, (*iii*) near complete channeling of glucose-derived pyruvate into the mitochondria, and (*iv*) a full reversal of lactate flux from production to consumption, likely due in part to the presence of oxidative stress. Also, the intracellular pool of GSH in different types of cells is described to be substantially (1–10 mM) in excess to keep an effective antioxidant defense (Franco et al., 2007), so a constant supply of NADPH is required when GSH is insufficient. NADPH is known to be a required intermediate for keeping a pool of reduced glutathione via glutathione reductase activity (Franco et al., 2007). Then, our data is further supporting the activation of GSH synthesis by the lower uptake rates of glucose sustained by the cells when extra lactic acid was co-fed, consequently, a lower supply of redox intermediate NADPH via oxidative PPP was expected. The glucose uptake rates

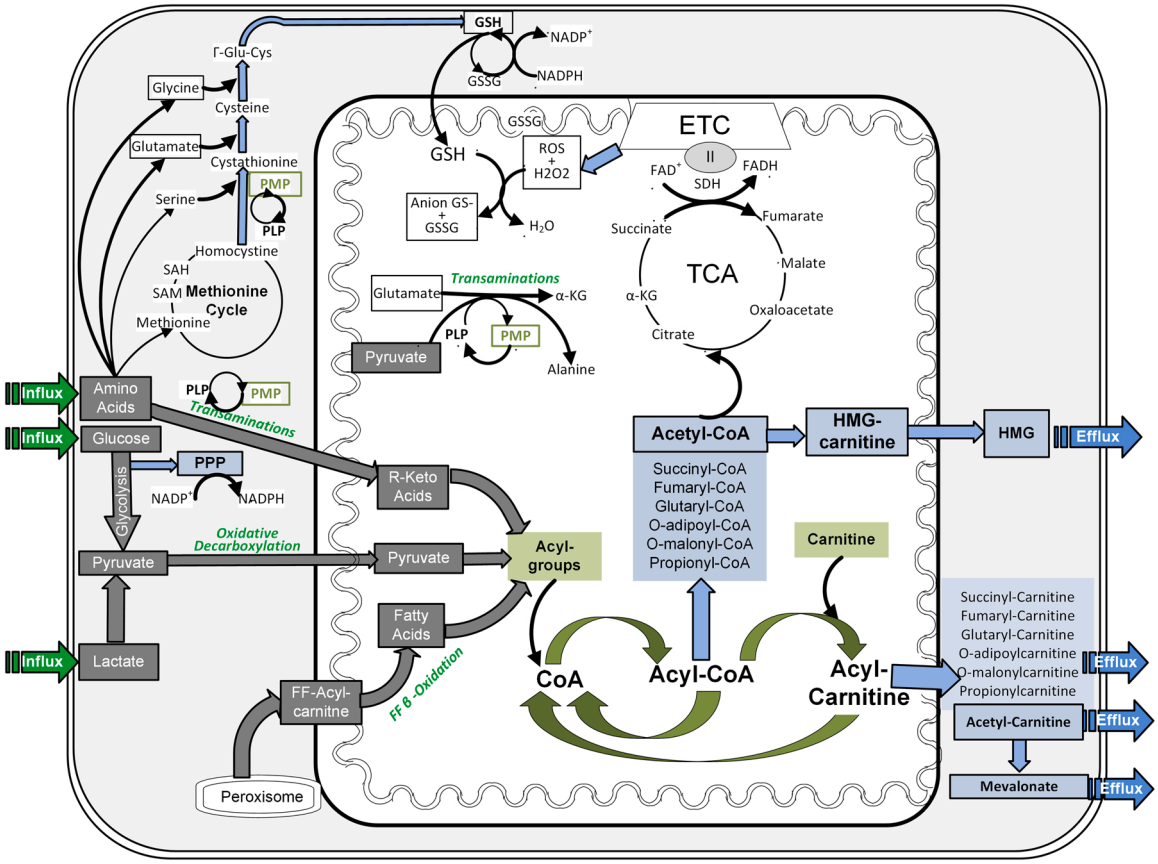

Fig. 11. Integrated diagram of metabolic pathways activated when CHO cells were fed with lactic acid and controlled at 2 g/L. Diagram shows the formation in the mitochondria of acyl-groups (green box) from amino acid influxes via their oxidative catabolism, from influxes of glucose and lactate to generate pyruvate via glycolysis and lactate oxidation, and from fatty acids via β-oxidation (grey boxes and grey arrows). Also showing the dynamic exchange for the homeostasis of both CoA/Acyl-CoA and Acyl-CoA/Acylcarnitine ratios (large, bolded names connected with green arrows) in the mitochondria. Then, Acyl-CoA mitochondrial pool used to: (i) supply the TCA cycle (blue boxes and arrows) and/or (ii) transfer the acyl-groups to carnitine (green box) to form acylcarnitines and so being translocated into the cytosol and further to the medium (blue boxes and blue arrows). Acetyl-CoA (bolded blue boxes) showing multiple destinies, consumed as TCA cycle intermediate, as substrate for the syntheses of HMG and mevalonate/mevalonolactone (bolded blue boxes and arrows). The methionine cycle, with the inputs of amino acids glycine, glutamic acid, and serine, contributes via the transsulfuration pathway (blue arrows) to produce reduced glutathione (GSH). Co-factor pyridoxamine 5-P (PMP in green letters and boxes) is key in the first step of GSH synthesis and the transamination catalyzed by the alanine/glutamate aminotransferase. At the electron-transport chain (ETC), the generation (blue arrows) of reactive-oxygen species (ROS), hydrogen peroxide (H_2O_2), and the presence of the enzyme complex II succinate dehydrogenase (SDH) are showing the interplay between the ETC/TCA cycle, oxidative stress by ROS and H_2O_2, and antioxidant defense exerted by GSH with the concomitant formation of the oxidated form GSSG and H_2O.

dropped by 39 % (from 1.02 to 0.63 mmol/cell/mL*day) from days 5–10 when lactic acid was controlled at 2 g/L, in comparison with control cultures (without lactic acid control) where those rates decreased by only 15 % (from 0.95 to 0.81 mmol/cell/mL*day) (Table S7 in Vappiani et al., 2021). In case of a shortage of NADPH, the transsulfuration pathway is activated to produce GSH to compensate for the NADPH shortage. This explanation is supported by the changes of relative rate profiles of PMP, glycine, and glutamic acid (Figs. 8 and 10). The higher demand of PMP could in part explain the active use of homocysteine from the methionine cycle to produce homocystathionine – the first step in the transsulfuration pathway (Fig. 11). Also, the increasing consumption rates of glycine and glutamic acid in later days of the cultures point to the same direction of active transsulfuration to produce GSH (Fig. 11). The final extracellular relative abundances of GSH were the same between the two treatments, an increasing secretion until day 10, when it started decreasing until day 17 (Supplementary Material, Fig. S1). While our culture conditions featured the same feeding regime and the same feed solutions, we still observed lower relative abundances of methionine throughout the culture time from day 5 onward (Fig. 5 in Vappiani et al., 2021), again supporting the possible active use of homocysteine in conjunction with increasing glycine and glutamic acid demands to synthetize GSH (Fig. 11).

Maximizing the secretory capacity of CHO cells to produce monoclonal antibodies (mAbs) necessitates high energy demands from cells. Consequently, an active metabolism can induce an influx of reactive oxygen species (ROS) within CHO cultures. Excessive generation of ROS can impair CHO culture performance in growth and/or productivity by oxidizing critical proteins and lipid membranes, creating lesions in DNA/RNA, and inducing apoptosis during oxidative stress. Furthermore, the accumulation of ROS such as superoxide radicals, hydroxyl radicals, and hydrogen peroxide (H_2O_2) can alter the redox state of cell cultures and yield an imbalance of antioxidants. The interplay between ROS generation and antioxidant capacity is represented by the GSH/GSSG, NAD^+/NADH and $NAPD^+$/NADPH ratios·H_2O_2 and oxygen superoxide radicals play intricate roles in mitochondrial signaling to the rest of the cell (Mailloux and Willmore, 2014). However, in large quantities, both H_2O_2 and oxygen superoxide radicals can be harmful. Evidence shows that an overproduction of oxygen superoxide radicals can lead to the disassembly of Fe-S clusters present in TCA enzymes such as aconitase (ACN), succinate dehydrogenase (SDH), fumarase (FUM), and ETC complex I (NADH dehydrogenase) (Read et al., 2021). In connection with this picture of re-wired metabolic rates, a deficient vitamin pyridoxamine (B6) status might either directly cause higher oxidative stress or might affect cysteine and GSH synthesis and,

consequently, the entire GSH-dependent antioxidant defense system (Cheng-Chin Hsu et al., 2015). Through the adaptation of CHO cells to an extra supply of lactic acid, we found the adjustments of metabolic rates of intermediates as surrogate indicators of which pathways were affected and how cells could mitigate possible oxidative stress impact on mitochondrial activities, especially on the TCA cycle and ETC. Those two pathways contribute to OXPHOS, which is highly demanded after day 5 ("metabolic shift") for cell growth and viability, and to keep the mAb expression and its secretion (Templeton et al., 2017). Our results support the theory that cells respond to (*i*) the debilitated antioxidant defense by synthetizing GSH via transsulfuration and (*ii*) the ROS signaling to the mitochondria by an extensive use of succinate to overcome the temporary reversible inhibition of TCA cycle and ETC enzymes/complexes.

5. Conclusion

In this study, we describe a case of metabolic rewiring exhibited by CHO cells in response to a single intervention - the addition of lactic acid to control its concentration at 2 g/L from day 5 until cultures ended. The rationale behind this experimental strategy was based on the potential benefit of improving the mitochondrial function from supplying extra lactic acid - specifically after the transition from aerobic glycolysis to OXPHOS. A group of carnitine derivatives, HMG, and mevalonate appeared as surrogate markers of different metabolic pathways to maintain OXPHOS despite the partial impairments of the TCA cycle during a cell's transition between growth phases. Furthermore, the analysis based on two different metrics comparing the cell-specific rates of selected metabolites, provide us deeper insights into the possible connection of two main events: *i*) oxidative stress and *ii*) the partially impaired TCA cycle and ETC. The metabolic rate changes in the time course of the culture from day 5 onward suggest the activation of GSH synthesis as an antioxidant response to a potential oxidative stress damage, and simultaneously, the activation of the carbon-buffering system to remove all those activated acyl-CoA groups from the mitochondria, and finally from the cells.

Then, a possibly debilitated antioxidant defense was triggered by a smaller NADPH's cytosolic pool, in order to keep the TCA cycle and ETC properly running while overcoming an imminent cellular damage by ROS, the intensified use of intermediates such as glycine, glutamate, and PMP, for glutathione synthesis, was required. Additionally, the results of the high secretion rates of carnitine derivatives point to an overwhelmed TCA cycle failing to process efficiently all the extra acetyl groups from pyruvate oxidation and other acyl groups derived from fatty acid β-oxidation and amino acid catabolism.

In summary, based on the results, we explain a possible metabolic adaptive response of CHO cells to a lowered antioxidant glutathione defense with a negative impact on the TCA cycle's processing capacity of all acyl-CoAs generated from oxidative metabolizations of pyruvate, amino acids, and fatty acids, as reflected in the high secretion rates of seven carnitine derivatives. Our results contribute to the understanding of mitochondrial dysfunctionality and oxidative stress, common metabolic features among cancer cells. We uncover new biomarkers indicating the proper mitochondrial activities of the TCA cycle and ETC, and homeostasis of the intermediates for the antioxidant defense, which are cancer-specific vulnerabilities.

Funding sources

This research did not receive any grant from funding agencies in the public, commercial, or not-for-profit sectors.

CRediT authorship contribution statement

Yu Luo: Formal analysis, Writing – review & editing. **Johanna Vappiani:** Data curation, Investigation. **Keegan Orzechowski:** Investigation, Writing – review & editing. **Pramthesh Patel:** Funding acquisition, Project administration. **Daniel Sevin:** Supervision, Writing – review & editing. **Juan Aon:** Conceptualization, Supervision, Writing – original draft, Writing – review & editing.

Declaration of Competing Interest

The authors declare the following financial interests/personal relationships which may be considered as potential competing interests: Juan Aon, Daniel Sevin, and Pramthesh Patel report a relationship with GlaxoSmithKline that includes equity or stocks.

Data Availability

The authors do not have permission to share data.

Acknowledgments

The authors would like to acknowledge Thomas Eyster for the comments on this manuscript. The authors would also like to acknowledge Sybille Galosy and Tim Boung Wook-Lee for the discussion and interpretation of results.

Appendix A. Supporting information

Supplementary data associated with this article can be found in the online version at doi:10.1016/j.jbiotec.2022.10.004.

References

Adeva-Andany, M.M., Calvo-Castro, I., Fernández-Fernández, C., Donapetry-García, C., Pedre-Piñeiro, A.M., 2017. Significance of L-carnitine for human health. IUBMB Life 69, 578–594. https://doi.org/10.1002/iub.1646.

Ahn, W.S., Antoniewicz, M.R., 2013. Parallel labeling experiments with [1,2–13C] glucose and [U-13C]glutamine provide new insights into CHO cell metabolism. Metab. Eng. 15, 34–47. https://doi.org/10.1016/j.ymben.2012.10.001.

Berni, A., Meschini, R., Filippi, S., Palitti, F., De Amicis, A., Chessa, L., 2008. L-Carnitine enhances resistance to oxidative stress by reducing DNA damage in Ataxia telangiectasia cells. Mutat. Res. Genet. Toxicol. Environ. Mutagen. 650, 165–174. https://doi.org/10.1016/j.mrgentox.2007.11.008.

Bistulfi, G., VanDette, E., Matsui, S.I., Smiraglia, D.J., 2010. Mild folate deficiency induces genetic and epigenetic instability and phenotype changes in prostate cancer cells. BMC Biol. 8, 6. https://doi.org/10.1186/1741-7007-8-6.

Brass, E.P., 1994. Overview of coenzyme A metabolism and its role in cellular toxicity. Chem. Biol. Interact. 90, 203–214. https://doi.org/10.1016/0009-2797(94)90010-8.

Console, L., Scalise, M., Mazza, T., Pochini, L., Galluccio, M., Giangregorio, N., Tonazzi, A., Indiveri, C., 2020. Carnitine traffic in cells. Front. Cell. Dev. Biol. 8, e583850 https://doi.org/10.3389/fcell.2020.583850.

Corbin, J.M., Ruiz-Echevarría, M.J., 2016. One-carbon metabolism in prostate cancer: the role of androgen signaling. Int. J. Mol. Sci. 17, 1208. https://doi.org/10.3390/ijms17081208.

Davies, M.N., Kjalarsdottir, L., Thompson, J.W., Dubois, L., Steves, R., Ilkayeva, O., Brosnan, M., Rolph, T., Grimsrud, P., Muoio, D., 2016. The acetyl group buffering action of carnitine acetyltransferase offsets macronutrient-induced lysine acetylation of mitochondrial proteins. Cell Rep. 14, 243–254. https://doi.org/10.1016/j.celrep.2015.12.030.

Ellis, B.A., Poynten, A., Lowy, A.J., Furler, S.M., Chisholm, D.J., Kraegen, E.W., Cooney, G.J., 2000. Long-chain acyl-CoA esters as indicators of lipid metabolism and insulin sensitivity in rat and human muscle. Am. J. Physiol. Endocrinol. Metab. 279, 554–560. https://doi.org/10.1152/ajpendo.2000.279.3.E554.

Eyster, T., Talwar, S., Fernandez, J., Foster, S., Hayes, J., Allen, R., Reidinger, S., Wan, B., Ji, X., Aon, J., Patel, P., Ritz, D., 2020. Tuning monoclonal antibody galactosylation using Raman spectroscopy-controlled lactic acid feeding. Biotechnol. Prog. 37, e3085 https://doi.org/10.1002/btpr.3085.

Franco, R., Schoneveld, O.J., Pappa, A., Panayiotidis, M.I., 2007. The central role of glutathione in the pathophysiology of human diseases. Arch. Physiol. Biochem 113, 234–258. https://doi.org/10.1080/13813450701661198.

Hsu, C.-C., Cheng, C.-H., Hsu, C.-L., Lee, W.-J., Huang, S.-C., Huang, Y.-C., 2015. Role of vitamin B6 status on antioxidant defenses, glutathione, and related enzyme activities in mice with homocysteine-induced oxidative stress. Food Nutr. Res. 59, 25702. https://doi.org/10.3402/fnr.v59.25702.

Hunter, W.G., Kelly, J.P., McGarrah, R.W., Khouri, M.G., Craig, D., Haynes, C., Ilkayeva, O., Stevens, R.D., Bain, J.R., Muehlbauer, M.J., Newgard, C.B., Felker, G. M., Hernandez, A.F., Velazquez, E.J., Kraus, W.E., Shah, S.H., 2016. Metabolomic profiling identifies novel circulating biomarkers of mitochondrial dysfunction differentially elevated in heart failure with preserved versus reduced ejection

fraction: evidence for shared metabolic impairments in clinical heart failure. J. Am. Heart Assoc. 5 (8) https://doi.org/10.1161/JAHA.115.003190.
Koppula, P., Zhang, Y., Shi, J., Li, W., Gan, B., 2017. The glutamate/cystine antiporter SLC7A11/xCT enhances cancer cell dependency on glucose by exporting glutamate. J. Biol. Chem. 292, 14240–14249. https://doi.org/10.1074/jbc.M117.798405.
Li, J., Wong, C.L., Vijayasankaran, N., Hudson, T., Amanullah, A., 2012. Feeding lactate for CHO cell culture processes: impact on culture metabolism and performance. Biotechnol. Bioeng. 109, 1173–1186. https://doi.org/10.1002/bit.24389.
Luo, J., Vijayasankaran, N., Autsen, J., Santuray, R., Hudson, T., Amanullah A. Li, F., 2012. Comparative metabolite analysis to understand lactate metabolism shift in Chinese hamster ovary cell culture process. Biotechnol. Bioeng. 109, 146–156. https://doi.org/10.1002/bit.23291.
Lyon, P., Strippoli, V., Fang, B., Cimmino, L.B., 2020. Vitamins and one-carbon metabolism: implications in human health and disease. Nutrients 12, 2867. https://doi.org/10.3390/nu12092867.
Mailloux, R.J., Willmore, W.G., 2014. S-glutathionylation reactions in mitochondrial function and disease. Front. Cell. Dev. Biol. 2, 68. https://doi.org/10.3389/fcell.2014.00068.
Mulukutla, B.C., Yongky, A., Daoutidis, P., Hu, W.-S., 2014. Bistability in glycolysis pathway as a physiological switch in energy metabolism. PLOS One 9, e98756. https://doi.org/10.1371/journal.pone.0098756.
Orsatti, L., Orsale, M.V., di Pasquale, P., Vecchi, A., Colaceci, F., Ciammaichella, A., Rossetti, I., Bonelli, F., Baumgaertel, K., Liu, K., Elbaum, D., Monteagudo, E., 2021. Turnover rate of coenzyme A in mouse brain and liver. PLoS One 16, e0251981. https://doi.org/10.1371/journal.pone.0251981.
Read, A.D., Bentley, R.E., Archer, S.L., Dunham-Snary, K.J., 2021. Mitochondrial iron-sulfur clusters: structure, function, and an emerging role in vascular biology. Redox Biol. 47, 102164 https://doi.org/10.1016/j.redox.2021.102164.
Reuter, S.E., Evans, A.M., 2012. Carnitine and Acylcarnitines. Clin. Pharmacokinet. 51, 553–572. https://doi.org/10.1007/BF03261931.
Sanderson, S.M., Gao, X., Dai, Z., Locasale, J.W., 2019. Methionine metabolism in health and cancer: a nexus of diet and precision medicine. Nat. Rev. Cancer 19, 625–637. https://doi.org/10.1038/s41568-019-0187-8.
Sengupta, N., Rose, S.T., Morgan, J.A., 2011. Metabolic flux analysis of CHO cell metabolism in the late non-growth phase. Biotechnol. Bioeng. 108, 82–92. https://doi.org/10.1002/bit.22890.
Shi, L., Tu, B.P., 2015. Acetyl-CoA and the regulation of metabolism: mechanisms and consequences. Curr. Opin. Cell Biol. 33, 125–131. https://doi.org/10.1016/j.ceb.2015.02.003.
Templeton, N., Dean, J., Reddy, P., Young, J.D., 2013. Peak antibody production is associated with increased oxidative metabolism in an industrially relevant fed-batch CHO cell culture. Biotechnol. Bioeng. 110, 2013–2024. https://doi.org/10.1002/bit.24858.
Templeton, N., Smith, K.D., McAtee-Preira, A.G., Dorai, H., Betenbaugh, M.J., Lang, S.E., Young, J.D., 2017. Application of 13C flux analysis to identify high-productivity CHO metabolic phenotypes. Metab. Eng. 43, 218–225. https://doi.org/10.1016/j.ymben.2017.01.008.
Tuttle, S., Stamato, T., Perez, M.L., Biaglow, J., 2000. Glucose-6-phosphate dehydrogenase and the oxidative pentose phosphate cycle protect cells against apoptosis induced by low doses of ionizing radiation. Radiat. Res. 153, 781–787. https://doi.org/10.1667/0033-7587(2000)153[0781:GPDATO]2.0.CO;2.
Vappiani, J., Eyster, T., Orzechowski, K., Ritz, D., Patel, P., Sévin, D., Aon, J., 2021. Exometabolome profiling reveals activation of the carnitine buffering pathway in fed-batch cultures of CHO cells co-fed with glucose and lactic acid. Biotechnol. Prog. 37, e3198 https://doi.org/10.1002/btpr.3198.
Vaz, F.M., Wanders, R.J.A., 2002. Carnitine biosynthesis in mammals. Biochem. J. 361, 417–429. https://doi.org/10.1042/0264-6021:3610417.
Voet, D., Voet, J.G., 1995. Biochemistry, second ed. John Wiley and Sons, New York.
Young, J.D., 2013. Metabolic flux rewiring in mammalian cell cultures. Curr. Opin. Biotechnol. 24, 1108–1115. https://doi.org/10.1016/j.copbio.2013.04.016.